nature communications

Article

https://doi.org/10.1038/s41467-025-60619-2

Deep evolution of carbonated magmas controls ocean island basalt chemistry

Received: 2 August 2024

Accepted: 29 May 2025

Published online: 06 June 2025

Check for updates

Junlong Yang[1], Chao Wang[2] ✉, Zhenmin Jin[2] & Zhicheng Jing[1] ✉

The composition of ocean island basalts (OIBs) is key to understanding mantle differentiation and quantifying intra-plate carbon outflux. Existing petrogenesis models fail to simultaneously reproduce the low SiO_2 and low SiO_2/FeO^T characteristics of alkalic OIBs and ignore melt-orthopyroxene reactions in the lithosphere that may further elevate the SiO_2 content of primary magmas. Here we show experimentally that high-degree (>50%) high-pressure crystallization of carbonated primary magmas at the base of lithosphere drastically reduces both the SiO_2 content and SiO_2/FeO^T ratio, due to the combined effects of clinopyroxene and garnet precipitation and carbonates dissolution. The major-element chemistry of alkalic OIBs can be quantitatively reproduced by considering varying degrees of crystallization, melt-orthopyroxene reactions, and source CO_2 content. Our results imply high intra-plate carbon outfluxes and support the observed association of low OIB SiO_2 contents with low mantle potential temperatures, as slower magma transport at lower temperatures leads to more extensive crystallization and reaction.

Ocean island basalts (OIBs) produced by intraplate volcanism exhibit a wide range of chemical compositions in contrast to the relatively uniform compositions for mid-ocean ridge basalts (MORBs) (Fig. 1). Most OIBs are characterized as alkalic basalts with lower SiO_2 (~37–50 wt%) and higher FeO^T (~8–17 wt%) contents than those of MORBs. Various melting models involving different source lithologies have been proposed to reproduce alkalic OIB chemistry, including partial melting of carbonated-peridotite[1–7] and pyroxenite[8–12], and reaction between eclogite-derived melt and peridotite[13–15]. In all these models, alkalic OIB compositions were directly linked to the partial melt formed from deep-seated mantle sources. The diverse compositions of alkalic OIBs were frequently explained by introducing various subducted slab materials to the source regions. However, none of these one-stage melting and reaction models can explain the genesis of alkalic OIBs with extremely low SiO_2 contents (<42 wt%) together with high FeO^T contents, or equivalently low SiO_2/FeO^T ratios, such as those observed in many samples from Trindade-Vitoria and Fernando de Noronha (Fig. 1). Olivine crystallization of these melts can explain the low SiO_2 contents at low MgO contents but not at low SiO_2/FeO^T ratios (Fig. 1).

Other than source melting, deep evolution processes of source magmas, including high-pressure crystallization in magma chambers at the base of the lithosphere[16–20] and magma-rock reactions[21–23] during magma migration through the lithosphere may have greatly modified the major element chemistry of the OIBs. Although it has been demonstrated that the deep crystallization of picritic magmas derived from peridotite melting can explain the genesis of Hawaiian tholeiitic OIB compositions[16], such process only produces basalt compositions with $SiO_2 > 43$ wt%. In addition, the subsequent transport of magmas through the lithosphere would inevitably increase the SiO_2 content of the silica-undersaturated magmas due to melt-orthopyroxene reactions before eruption[22,24], posing a persistent challenge in explaining the low SiO_2 and low SiO_2/FeO^T characteristics of alkalic OIBs.

Although the presence of CO_2 has been linked to alkalic OIB formation by several observations, including the associations of OIBs with carbonatites[25], the presence of phenocrysts containing CO_2-rich melt inclusions[26], and xenoliths showing carbonatite metasomatism[27], its role in affecting magma evolution has often been overlooked, possibly due to the belief that melt-rock reactions occur at depths shallower than ~60 km, where magmas were usually assumed to have

[1]Department of Earth and Space Sciences, Southern University of Science and Technology, 518055, Shenzhen, China. [2]State Key Laboratory of Geological Processes and Mineral Resources, School of Earth Sciences, China University of Geosciences, 430074, Wuhan, China. ✉e-mail: wangchao@cug.edu.cn; jingzc@sustech.edu.cn

https://doi.org/10.1038/s41467-025-60619-2

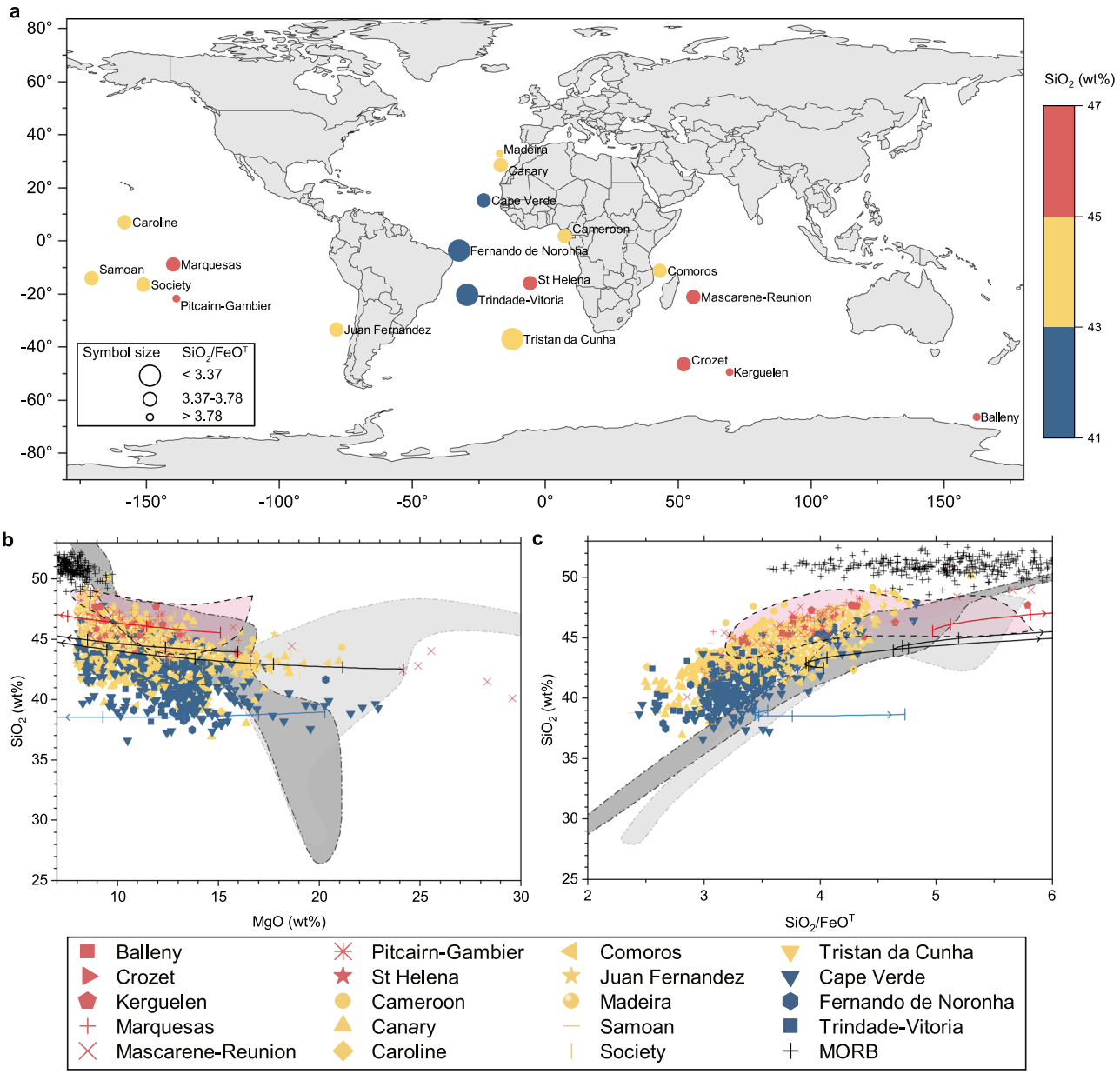

Fig. 1 | Global intraplate OIB volcanism and compositions of alkalic OIB lavas. **a** Map of global OIB eruption locations. The base map was generated using the Origin software (https://www.originlab.com/). The symbol color indicates the mean SiO_2 content of each individual ocean island and the symbol size represents the SiO_2/FeO^T ratio. **b** MgO and SiO_2 contents of OIBs and MORBs. **c** SiO_2/FeO^T ratios and SiO_2 contents of OIBs and MORBs. The data for alkalic OIB lavas are from ref. 35, in which only OIBs with MgO ≥8 wt% were selected to minimize alterations in melt compositions caused by clinopyroxene fractionation. The data for MORBs are from the GEOROC database (https://georoc.mpch-mainz.gwdg.de//georoc/). The light gray area enclosed by the dash-dot-dot line, pink area by the dashed line, and dark gray area by the dash-dot line represent the composition ranges of partial melts of carbonated-peridotite[1], partial melts of pyroxenite[8,9,11,12], and melts after reaction between eclogite-derived melt and peridotite[13–15], respectively. The black, red, and blue solid lines represent the evolution paths of melt compositions due to olivine crystallization for various starting melt compositions, calculated using the model of ref. 51. Each cross on the solid lines represents 10% olivine crystallization and the arrows represent the directions of olivine crystallization. The alkalic OIBs have lower SiO_2 contents and lower SiO_2/FeO^T ratios than those of MORBs and have lower SiO_2/FeO^T ratios at given SiO_2 contents than those of inferred silica-poor primary melts (see text) with SiO_2 <~42 wt%.

decarbonated[28,29]. But in fact, the CO_2 solubility in silica-undersaturated melt can be as high as ~2–10 wt% at ~30 km depth[30].

Here we propose that the involvement of CO_2 in the deep evolution processes of picritic magmas is the major factor controlling OIB chemistry. We report results from high-pressure crystallization and reaction experiments in CO_2-bearing systems and quantify the chemical evolution of carbonated magmas beneath various ocean islands. We demonstrate that although the presence of CO_2 does not inhibit melt-lithosphere reactions, which moderately increase magma SiO_2 content during ascent, it significantly modifies the crystallization behavior of deep-seated magmas, producing magmas with low SiO_2 and high FeO^T contents that are consistent with the alkalic OIB observations.

Results and discussion

High-pressure (HP) crystallization experiments of primary magmas (a picritic melt with MgO less than ~20 wt%) were performed at conditions of 3 GPa and 1150–1350 °C in a multi-anvil press (Methods and Supplementary Fig. 1) to investigate the evolution of melt composition upon crystallization in magma chambers beneath the lithosphere-

asthenosphere boundary (LAB). As the mantle is predominantly composed of peridotite component, we chose a carbonated picrite composition (CP-2) with a CO_2 content of ~6.6 wt% (Supplementary Table 1) as our starting material representing the primary melt formed by the partial melting of carbonated peridotite with 1.0 wt% CO_2 (ref. 1, Supplementary Text 1). Our experimental results show that clinopyroxene and garnet are the two liquidus phases that first precipitated from carbonated primary magmas during equilibrium crystallization (Supplementary Fig. 2), consistent with previous experimental results on carbon-free systems that garnet and pyroxene are major residual phases at pressures greater than ~2 GPa (refs. 12,31). Pressure and composition are the controlling factors for the crystallization of clinopyroxene and garnet rather than olivine. As temperature decreases, the total modal proportion of the two precipitating phases (defined as crystallization fraction, CF) increases gradually up to 80% at 1150 °C, whereas a small fraction of carbonate-rich melt (≤2.5 wt%) was observed to be in coexistence with the carbonated silicate melt for most temperatures (Supplementary Fig. 3). The residual silicate melt (hereafter referred to as HP-derived melt) shows a decreasing SiO_2 content from ~42 wt% for CP-2 to 20 wt% at a CF of ~80% with decreasing temperature, accompanied by an increase in CO_2 content in the melt from ~6.6 wt% to 32 wt% (Supplementary Fig. 4). The significant reduction in SiO_2 content is partly due to the crystallization of clinopyroxene and garnet similar to the CO_2-free case[16], and partly due to the strong dilution effect of the carbonated components dissolved in the melt. Upon HP-crystallization, the concentrations of dissolved CO_3^{2-} ions and the associated Ca^{2+}, Mg^{2+}, and Fe^{2+} cations (ref. 32) in the HP-derived melt would increase due to the incompatible nature of carbonates[33], resulting in a strong negative correlation between the SiO_2 and CO_2 contents in the melt as seen in Supplementary Fig. 4 and ref. 1. The ascending of CO_2-bearing magmas to shallow depths would release gaseous CO_2 before eruption and leave the associated cations in the residual melt, thereby effectively diluting the SiO_2 content in the finally erupted basalts. To account for such decarbonation process, the SiO_2 contents in HP-derived melts were normalized on the CO_2-free basis as $\bar{X}_{SiO_2} = X_{SiO_2}/(1 - X_{CO_2})$. The resulted $\bar{X}_{SiO_2}$ ranges from ~45 wt% for CP-2 to ~30 wt% at a CF of ~80% (Fig. 2). The composition range defined by CP-2 and HP-derived melt covers the SiO_2 content range (~36–45 wt%) for the alkalic OIBs at similar MgO contents (~16–18 wt%), confirming the critical role of CO_2 in HP-crystallization.

Moreover, no olivine, the most MgO- and FeO^T-rich mineral in the upper mantle, crystallizes from the melt at high pressure. Thus, the overall effect of high-pressure crystallization of garnet and clinopyroxene and CO_2 enrichment is that, on the CO_2-free basis, the SiO_2 and Al_2O_3 contents decrease, the CaO and FeO^T contents increase, and the MgO content remains nearly constant due to the additional Mg-Fe redistribution between minerals and melt (Figs. 2–3 and Supplementary Fig. 5). The FeO^T content and SiO_2/FeO^T ratio in the HP-derived melt change from ~10 wt% and ~4.7 for CP-2 to ~17 wt% and ~1.75 for the HP-derived melt, respectively, also covering the FeO^T content and SiO_2/FeO^T ratio ranges for alkalic OIBs (Fig. 2). Therefore, our experimental results demonstrate that the composition evolution of the primary melts towards SiO_2-poor and FeO^T-rich directions by high-pressure crystallization is strongly enhanced by the presence of CO_2 in the silicate melt.

We also performed melt-lithosphere reaction experiments for CO_2-bearing melts at 1 GPa and 1200 °C in a piston-cylinder apparatus (Methods). We investigated two different starting melt compositions: CP-2M with a CO_2 content of ~10 wt% (Supplementary Table 2) has a composition close to that of the HP-derived melt, representing the derived melt at ~70% CF from the primary melt CP-2; CP-2 is the same carbonated picrite used in HP crystallization experiments, representing the ascended primary magma without experiencing any crystallization. In each experiment, either CP-2M or CP-2 was placed in contact with a natural orthopyroxene aggregate (Supplementary Fig. 1b) to enable chemical reactions along the contact interface. Orthopyroxene was used here to represent the lithospheric mantle, as previous studies have demonstrated that the interaction between silica-deficient melt and the lithospheric peridotite occurs predominantly through melt-orthopyroxene reactions[21,22]. Olivine, if present, would increase the Mg# of the melt[34] though Mg-Fe exchange reactions between olivine and melt, but would not affect the SiO_2 content of the melt. In addition, a similar Mg-Fe exchange also occurs between orthopyroxene and melt[34], resembling the effect of olivine. Thus, using orthopyroxene to represent the lithosphere would not affect our results but help better characterize the melt-lithosphere reactions. Our experimental results demonstrate that both the primary melt and the HP-derived melt in the presence of CO_2 would react with orthopyroxene to produce olivine precipitates through the reaction of silica-deficient melt + orthopyroxene = silica-rich melt + olivine (refs. 21,22), with clinopyroxene as a byproduct. It should be noted that olivine crystals in the recovered sample charges contain both precipitated ones through melt-orthopyroxene reaction and crystallized ones from melt due to decreasing temperature at relatively low pressure. It is neither needed nor possible to distinguish these olivine crystals because in either case they are equilibrium minerals with the coexisting melt (hereafter referred to as evolved melt). Effectively, we can simplify the melt-orthopyroxene reaction as orthopyroxene assimilation reaction (silica-deficient melt + orthopyroxene = silica-rich melt) and attribute all olivine produced in the experiments to crystallization. Then the composition of the evolved melt would be equivalent to that of the parental melt of OIBs before the final olivine crystallization at near surface depths. The reaction process drives the compositions of both CP-2 and CP-2M toward silica-rich and iron-deficient directions and the evolved melt compositions can reach ~48 wt% SiO_2 and ~9 wt% FeO^T with an SiO_2/FeO^T ratio of ~5.2 (CP-2 reacted melt) and ~50 wt% SiO_2 and ~8 wt% FeO^T with an SiO_2/FeO^T ratio of ~6.0 (CP-2M reacted melt) at various reaction fractions (RF, defined as the mass percentage of orthopyroxene absorbed into the system). Thus, if the CO_2-bearing primary magmas ascend directly after formation, they would unlikely preserve their source SiO_2 content levels after melt-orthopyroxene reactions and would likely result in lower FeO^T contents than those of OIBs. In contrast, the composition of the evolved melts after various degrees of high-pressure crystallization and melt-orthopyroxene reaction can cover the entire SiO_2 and FeO^T content ranges of alkalic OIBs simultaneously (Fig. 2). The evolution paths of other major oxide components than SiO_2 and FeO^T are also consistent with the compositions of alkalic OIBs (Supplementary Text 2 and Supplementary Fig. 6).

Here we present a parameterized model based on our experimental results and previous experimental results on CO_2-free picritic melts[16] to quantify the effects of high-pressure crystallization and melt-orthopyroxene reaction on the major element chemistry of alkalic OIBs (Methods). In this model, the normalized content of a major component $\bar{X}_i^{Calc}$ (i = SiO_2, MgO, FeO^T, or Al_2O_3) in the evolved magma is expressed as a function of CF, RF, and the CO_2 content in the peridotite-derived primary melt ($X_{CO_2}^{Pri}$), with model parameters fitted to experimental results. Using our model, we evaluated the contributions of various factors of deep evolution processes to reproducing the compositions of alkalic OIBs. The estimated parental melt compositions[35] by adding olivine to OIB compositions were used as target compositions ($\bar{X}_i^{Target}$) of the evolved magmas after high-pressure crystallization and melt-lithosphere reaction but before olivine crystallization close to the surface. For each OIB composition, the sum of squared residuals between the calculated contents and the target ones ($\sum_i (\bar{X}_i^{Calc} - \bar{X}_i^{Target})^2$) was minimized to find solutions for CF, RF, and $X_{CO_2}^{Pri}$. The results were grouped and averaged for each

https://doi.org/10.1038/s41467-025-60619-2

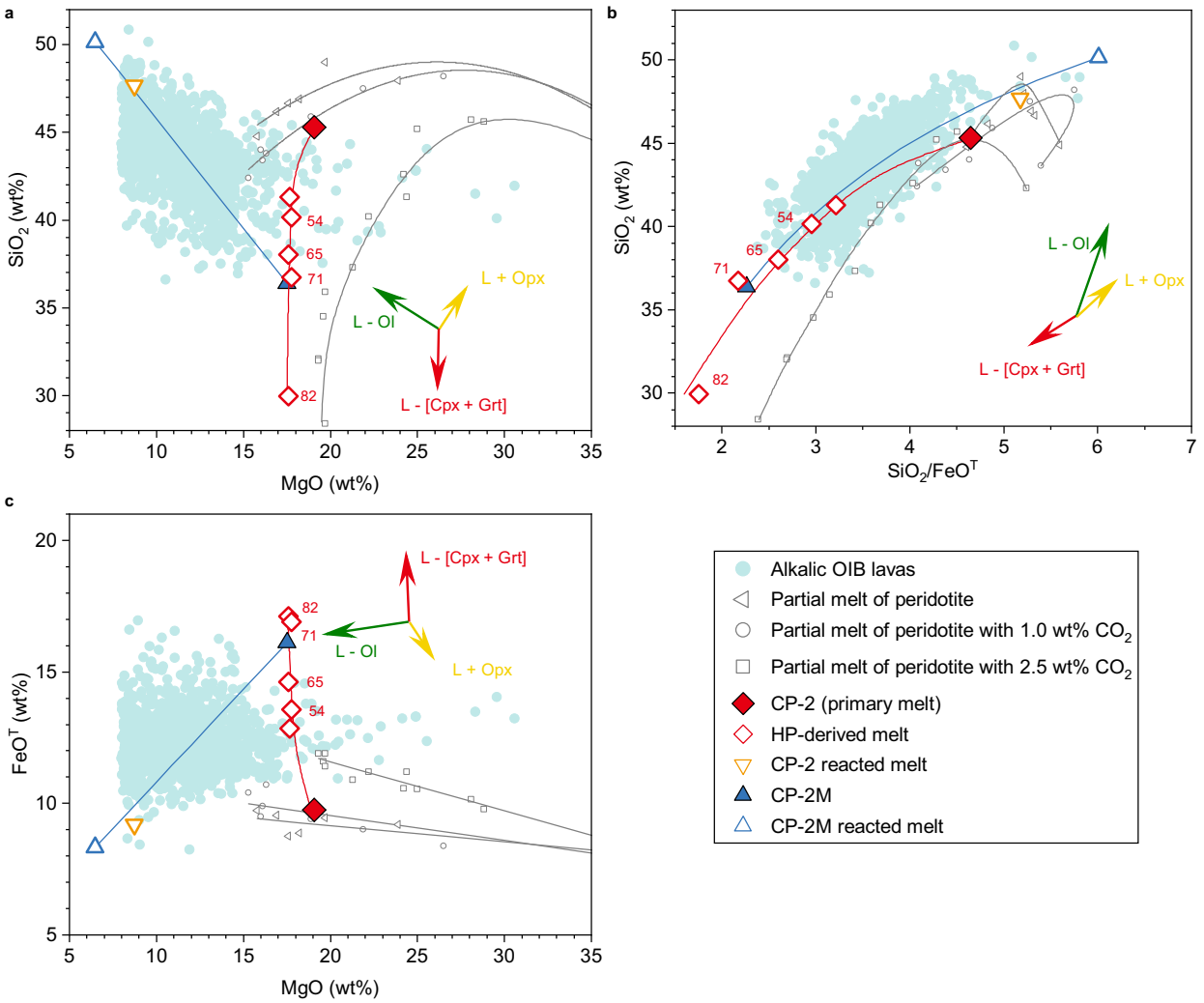

Fig. 2 | The composition evolution of carbonated alkalic OIB magmas. a SiO_2-MgO relations. **b** SiO_2-SiO_2/FeO^T relations; and (**c**) FeO^T-MgO relations. In each subplot, grey symbols with grey trendlines represent the compositions of primary magmas derived from partial melting of carbon-free peridotite[52,53] at 3 GPa and 1430-1630 °C and carbonated peridotite[1] at 3 GPa and 1350-1600 °C. The red solid diamond (CP-2) represents the primary melt (picritic melt) formed by the partial melting of carbonated peridotite with 1.0 wt% CO_2 (ref. 1) at 1450 °C and was selected as the starting composition in our high-pressure (HP) crystallization experiments. The red diamonds as guided by the red line represent HP-derived melts at various crystallization fractions (shown as percentage numbers next to the data points) of the carbonated picritic melt (CP-2). Both the CP-2M composition (blue solid triangle), representing a typical HP-derived melt, and the CP-2 composition, representing a primary magma without experiencing crystallization, were used as the starting compositions for melt-orthopyroxene reaction experiments. The blue empty triangle and the orange empty triangle represent the compositions after melt-orthopyroxene reactions at shallow lithosphere conditions (see text) from CP-2M (as guided by the blue line) and CP-2, respectively. The compositions of alkalic OIB lavas (cyan) are the same as those plotted in Figs. 1b, c. Arrows indicate the evolving directions of HP crystallization of clinopyroxene and garnet (Cpx and Grt, red), orthopyroxene (Opx) assimilation (yellow), and olivine (Ol) fractionation (green).

individual ocean island (Supplementary Table 3) and are compared with the compositions of the OIBs in Fig. 4 and Supplementary Fig. 7.

Results show that most alkalic OIBs underwent ~57–97% crystallization at high pressure and ~17–47% reaction with orthopyroxene, and had ~1.9–4.9 wt% CO_2 in their primary magmas (Fig. 4). Comparing the calculated CO_2 contents in primary magmas from our model and that of source regions[36], the primary magmas can be reproduced by ~8–20% partial melting of an enriched mantle source with ~0.4 wt% CO_2, close to the high-end estimate for CO_2 content in the source regions of intraplate OIBs[36]. Alternatively, these primary magmas can also be formed by higher degrees of melting (~10–30%) of a mantle source with relatively lower CO_2 but mixed with a small amount (<10%) of CO_2-rich subducted materials (e.g., GLOSS[35] with CO_2 content of ~3 wt%). Such addition of limited subducted materials is consistent with TiO_2 enrichment constraints on the formation of alkalic OIBs[37], but would not significantly affect the contents of other major components (Supplementary Text 3 and Supplementary Table 4). The ~10-30% degrees of source melting are consistent with petrological estimates[38,39]. As shown in Fig. 4, the composition characteristics of OIBs (e.g., $\bar{X}_{SiO_2}$, $\bar{X}_{FeO^T}$, and SiO_2/FeO^T ratio) and factors controlling evolution (CF, RF, and $X^{Pri}_{CO_2}$) are all correlated with each other. It is worth noting that the averaged SiO_2/FeO^T ratio of individual ocean island basalts shows a nearly linear relationship with CF (Fig. 4c), supporting our hypothesis that the deep evolution of carbonated magmas controls alkalic ocean island basalt chemistry. For alkalic OIBs with lower SiO_2 and higher FeO^T contents, they are likely formed by higher CF and RF during magma evolution and with higher CO_2 contents in the primary melt.

Our magma evolution model does not exclude proposals that heterogeneous materials were involved in the OIB sources as either

https://doi.org/10.1038/s41467-025-60619-2

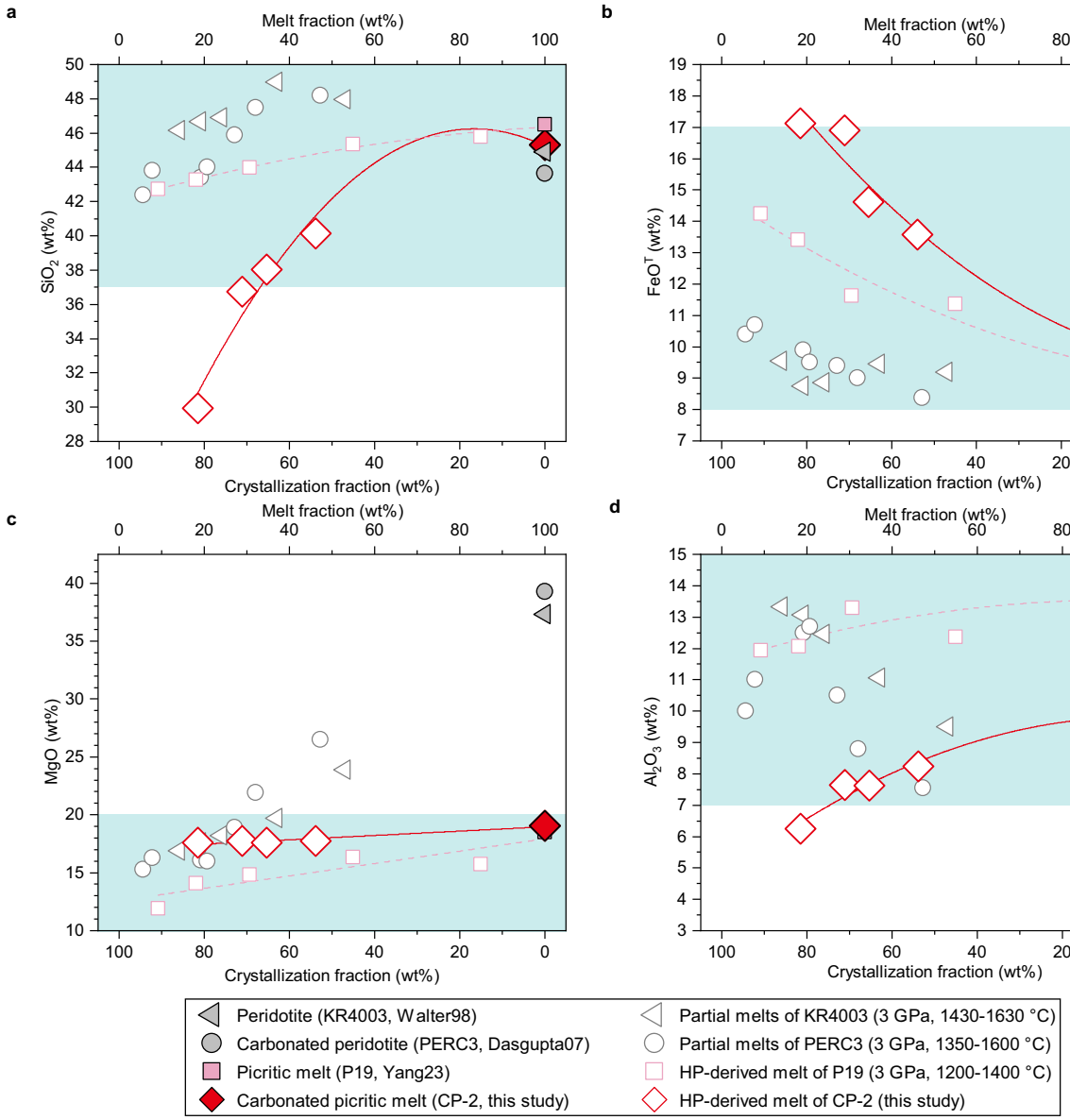

Fig. 3 | Effects of high-pressure crystallization on magma compositions as functions of crystallization fraction (CF). a SiO_2, **b** FeO^T, **c** MgO, and **d** Al_2O_3 contents of the magmas. Experimental data of high-pressure crystallization of carbonated picritic melt (red diamonds, this study) and CO_2-free picritic melt (pink squares, Yang23, ref. 16) are plotted, with sample labels, references, and experimental conditions listed in the legend. The solid and empty symbols represent the starting bulk compositions and the corresponding derived melts upon melting or crystallization, respectively. Red solid lines and pink dash lines represent the polynomial fitting for SiO_2, FeO^T, and Al_2O_3 contents and the linear fitting for MgO content as functions of CF (Methods). Partial melts of carbon-free peridotite (grey triangles, Walter98, ref. 52) and carbonated peridotite (grey circles, Dasgupta07, ref. 1) are shown for comparison. The starting bulk compositions of KR4003, RERC3, and P19 are listed in Supplementary Table 6. The cyan shaded areas represent the ranges of alkalic OIB compositions[35]. Compared to HP-crystallization of CO_2-free picritic magma or partial melting of CO_2-free or CO_2-bearing peridotites, high-pressure crystallization of carbonated picritic magma has the strongest effects on decreasing SiO_2 content and increasing FeO^T content with increasing crystallization fraction.

part of lithologies[8,40] or as melts[5] that can enrich the peridotitic mantle according to the OIB trace element and/or isotopic features, but emphasizes on the critical role of deep magma evolution processes on modifying the major element chemistry of OIBs. In fact, explaining the trace element and isotopic signatures of OIBs require only a small amount of additive materials such as those from subduction, which would not significantly affect the major element chemistry. Even for a highly altered mantle source, its derived primary melt is likely undersaturated in SiO_2 and rich in CO_2 and thus would undergo similar HP-crystallization and reaction processes, resulting in similar major element compositions. The relatively enriched features of alkalic OIBs compared to MORBs (e.g., $(La/Yb)_N \gg 1$) are usually linked to the presence of recycled materials and very low degrees of melting of source lithologies. Alternatively, the elevated $(La/Yb)_N$ ratios can be a result of high degrees of garnet crystallization near the LAB (Supplementary Fig. 8), alleviating the requirements for low melting degrees. Therefore, our deep magma evolution model of alkalic OIBs with high degrees of HP-crystallization after 10-30% partial melting of mantle peridotite can reconcile the discrepancies regarding the degrees of melting between geochemical estimations based on trace element chemistry[35,37] and petrological/geophysical estimations based on melting experiments and mantle potential temperature observations[39,41].

Geographically, the alkalic OIBs with lower SiO_2 content than 42 wt% are mostly located above the Atlantic Ocean basin (Fig. 1a). It has been determined seismically that these ocean islands have

https://doi.org/10.1038/s41467-025-60619-2

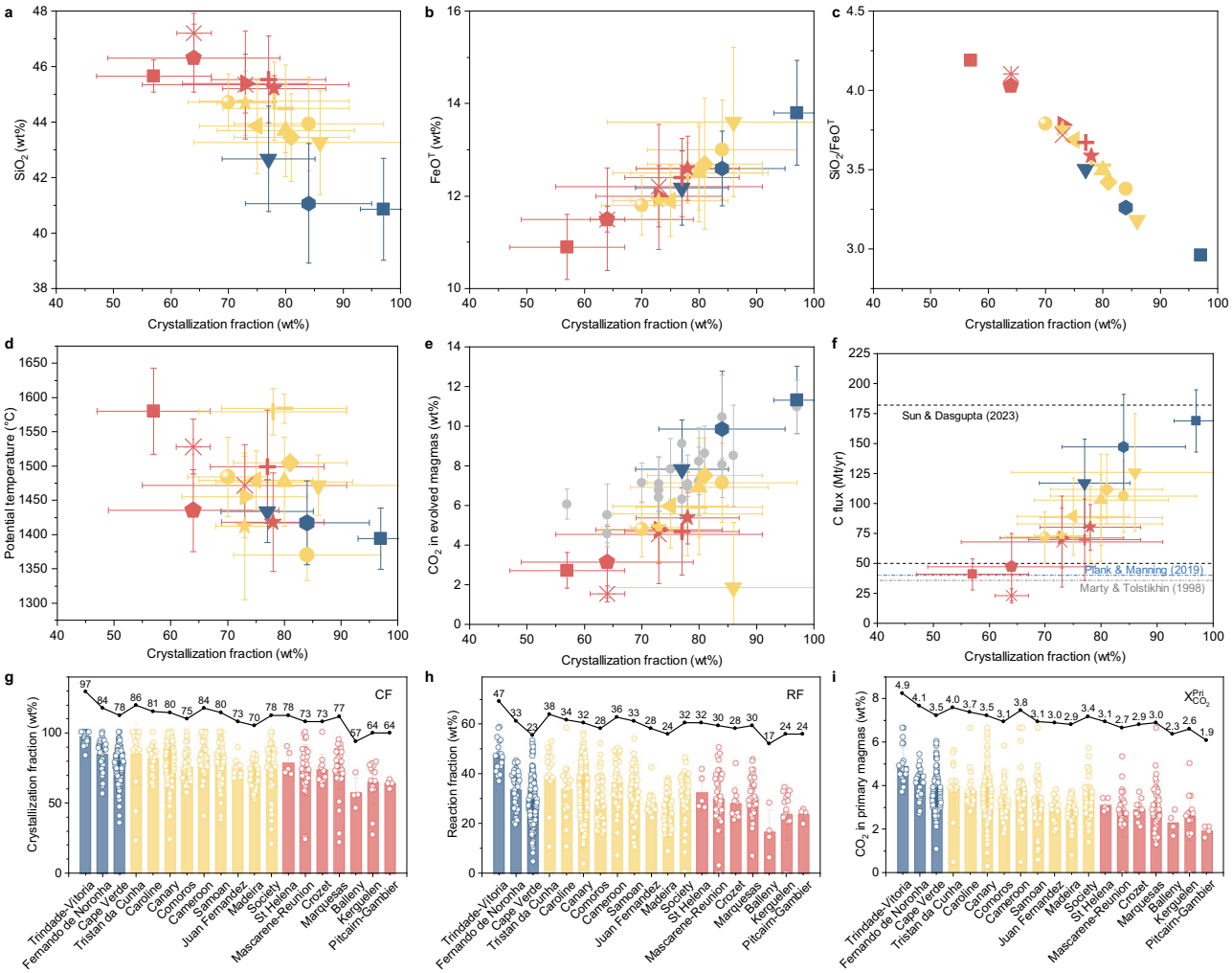

Fig. 4 | Correlations of alkalic OIB chemistry with degree of high-pressure crystallization. a SiO_2 content (**b**) FeO^T content, and (**c**) SiO_2/FeO^T ratio averaged for basalt samples from each individual ocean island (ref. 35. and Supplementary Table 3). **d** Mantle potential temperature estimated by ref. 41 using seismic observations. **e** Calculated CO_2 contents in evolved magmas after high-pressure crystallization and melt-orthopyroxene reaction, using the SiO_2-CO_2 correlation in Supplementary Fig. 4. Grey dots, shown for comparison, represent CO_2 contents of individual island groups estimated by ref. 35 according to the averaged Nb or Ba concentrations in their parental melts. **f** Carbon flux for each island group, calculated based on the CO_2 content in evolved magmas. The C fluxes estimated in this study are higher than that inferred by ref. 46 (blue dashed-dot line) and ref. 54 (grey dashed-dot-dot line), but located within the inferred ranges by ref. 35 (black dashed lines). Symbols in (**a**–**f**) are the same as those in Fig. 1. **g**–**i** Factors controlling magma evolution for each island based on our parameterized model. The bar diagrams with numbers above represent mean values of CF (**g**), RF (**h**), or $X^{Pri}_{CO_2}$ (**i**). The error bars represent one-standard deviations. The dots in the bars represent the probability density of CF, RF, or $X^{Pri}_{CO_2}$. Data on alkalic OIB lavas are the same those as listed in Fig. 1. From left to right, ocean islands are arranged in order of decreasing averaged SiO_2, with the same color coding for SiO_2 contents as in Fig. 1.

relatively lower mantle potential temperatures (T_p) (ref. 41), possibly because that these hotspots are fed by passive upwellings[42] or the plumes are trapped and cooled by small-scale convection in the upper mantle[43]. The correlation between OIB SiO_2 and FeO^T contents and the corresponding mantle potential temperatures (Supplementary Fig. 9) implies that lower T_p likely promotes both high-pressure crystallization and melt-orthopyroxene reaction (Fig. 4) and hence results in lower SiO_2 and higher FeO^T contents for the erupted OIBs. Such correlation between T_p and CF becomes more apparent when only OIB data with LAB depths (lithospheric thickness) greater than ~66 km are considered, when high-pressure crystallization of garnet and clinopyroxene likely occurs (Supplementary Text 4 and Supplementary Fig. 10). In contrast, the CF and hence OIB SiO_2 and FeO^T contents do not show obvious correlation with the LAB depth, even for OIBs with LAB depths greater than ~66 km (Supplementary Fig. 10d). The correlation between CF and T_p (Supplementary Fig. 10c) may be explained by the differences in time durations for magma accumulation beneath LAB and its ascending in the lithosphere at different mantle potential temperatures. At a relatively low T_p, the viscosity of magma is high, suggesting low mobility of the magma in the lithosphere. Thus, magmas for ocean islands with lower mantle potential temperatures likely stay in the deep magma chambers and in the lithosphere for longer durations and in turn would experience higher extent of crystallization and melt-lithosphere reaction.

Based on our parameterized model, the estimated CO_2 contents (Fig. 4e and Supplementary Table 5) in the evolved magmas after high-pressure crystallization and melt-lithosphere reaction processes are in the range of ~2–11 wt%. These estimates are consistent with those obtained by the liquid-based thermobarometer[35] and Nb and Ba concentrations which are often used as reliable proxies to trace CO_2 in mantle melts prior to degassing[35,44] (Fig. 4e). Taking the plume magma production rates (~2 km^3/yr) inferred by ref. 45 and the CO_2 contents of the evolved OIB melts from this study (Supplementary Table 5), the calculated carbon (C) outflux at ocean islands ranges from ~20 to ~170 Mt/yr, which is significantly greater than the estimated value of ~36 Mt/yr based on the $CO_2/^3He$ ratio and ^3He flux, but is comparable to

the recent estimate (50–182 Mt/yr) by ref. 35. (Fig. 4f). Given the estimated C inputs during subduction (~82 Mt/yr) and MORB/Arcs outputs (~39 Mt/yr) from ref. 46, our high C flux (~20–170 Mt/yr) estimated based on CO_2 in OIB evolved magmas before eruption implies either a net outflux of C from the Earth's interior (~0–130 Mt/yr) or hidden storage of outgassed C in the lithosphere[35].

Methods

Starting materials

There are two types of starting materials in this study: carbonated picrite with ~19 wt% MgO, representing the partial melt of carbonated peridotite (CP-2; Supplementary Tables 1) and the derived melt from high-pressure crystallization of CP-2 (CP-2M; Supplementary Table 2).

The CP-2 and CP-2M compositions were prepared by mixing appropriate amounts of high-purity reagent powders (SiO_2, TiO_2, MgO, Al_2O_3, MnO, Cr_2O_3, $CaCO_3$, Na_2CO_3, K_2CO_3) with natural dolomite. The oxides and carbonates were preheated at 1000 °C and 400 °C, respectively, for 10 h to remove adsorbed water and then stored in an oven at 150 °C. After mixing the reagent components under ethanol in an agate mortar for 6 hours, the mixtures were dried, cold-pressed into pellets, and then loaded into Pt crucibles for melting in a high-temperature box furnace. For the mixtures with CP-2 and CP-2M compositions, glasses were prepared to facilitate equilibration during high-pressure experiments. The mixtures were gradually heated to 1650 °C in air and kept for 30 min to ensure melting, before quenching into glasses by submerging into water. The glasses were ground in agate mortars for several hours and heated at 800 °C for 12 h to remove possible absorbed water during quench. The FeO component was added to glasses as high-purity FeO powder (99.5%, Alfa Aesar) to avoid oxidation of Fe^{2+} to Fe^{3+} during the synthesis process. The final mixture powders were ground again in an agate mortar for several hours under ethanol and dried for more than 24 h in a 150 °C oven.

Experimental methods

Two series of experiments, reaction or melting, were conducted in this study. The melt-orthopyroxene reaction experiments were conducted at 1.0 GPa using piston-cylinder press[47] at Southern University of Science and Technology. In these experiments, the cell assembly consists of a Au_{75}-Pd_{25} sample capsule, which is sandwiched between two MgO rods, a graphite sleeve furnace, a Pyrex glass sleeve, and a salt sleeve. Starting materials with CP-2 or CP-2M compositions were loaded in a graphite cup with inner diameter (ID) of 1.5 mm and height (H) of 2.0 mm. The graphite cup was subsequently placed in the bottom half of the Au_{75}-Pd_{25} capsule with ID of 2.6 mm, outer diameter (OD) of 3.0 mm, and H of 4.4 mm. A layer of compressed orthopyroxene powders with OD of 2.6 mm and H of 2.0 mm was placed above the graphite cup in the top half of the Au_{75}-Pd_{25} capsule, before sealing by a laser welding machine (Supplementary Fig. 1b).

The high-pressure crystallization experiments, or equivalently melting experiments, were conducted at 3.0 GPa in a double-stage 6-8 type multi-anvil press at Southern University of Science and Technology. Tungsten carbide cubes with 25.4 mm edge length and 12 mm truncated edge length and Cr-doped MgO octahedral pressure medium with 18 mm edge length were used for the experiments (18/12 cell assembly), similar to those used in ref. 16. The starting materials (CP-2) was encapsulated within graphite capsules with ID of 1.5 mm and H of 2.6 mm, which were subsequently placed into the Pt capsules with ID of 2.6 mm, OD of 3.0 mm, and H of 3.0 mm. A layer of glassy carbon spheres was loaded in the top half of the graphite capsule (Supplementary Fig. 1a) to extract melt for precise composition measurements[48–50]. The capsules were heated to 200 °C in a vacuum oven for 12 h to keep samples from absorbing water, before final sealing by a laser welding machine. The use of carbon spheres can help separate partial melts from coexisting crystals, thereby providing relatively large and well-defined areas of melts for chemical analyses and preventing reactions between melts and crystals during quench[50]. No metallic iron was observed in the run products indicating the carbon spheres and graphite capsules were not oxidized through the reaction of 2FeO (melt) + C = 2Fe (metal) + CO_2 (melt) to become dissolved in the melts.

Type C thermocouple ($W_{95}Re_5$-$W_{74}Re_{26}$) was used to monitor temperatures in both series of experiments. Uncertainties in temperatures are expected to be less than 25 °C based on calibration experiments for the temperature gradient across the samples (Supplementary Text 5 and Supplementary Fig. 11). Pressures of the experiments were determined using the pre-calibrated load-pressure relationships. Uncertainties in pressures are estimated to be 0.1–0.3 GPa (or <10% for relative uncertainties in pressure). Experiments were terminated by turning off the heating power. The recovered sample charges were sectioned parallel to the cylindrical axis and then polished to exposed run products. Carbon spheres, once exposed, were carefully protected with some extra epoxy coating to prevent dragging during subsequent polishing processes.

Analytical methods

Microstructures of the recovered samples were examined using a ZEISS Sigma 300 scanning electron microscope (SEM) at Southern University of Science and Technology. Quantitative analyses of major element compositions of minerals and melts were conducted using a JXA-8230 electron microprobe at Wuhan SampleSolution Analytical Technology Co., Ltd. The analyses were conducted using an accelerating voltage of 15 kV. For minerals, a beam size of 1-5 μm and a beam current of 15 nA were used, whereas for quenched melts, a large beam size of 10-20 μm and a reduced beam current of 10 nA were used. The acquired data were corrected using a modified ZAF (atomic number, absorption, fluorescence) correction procedure. The following standards were used for quantitative analyses of the major elements: Jadeite for Na; Rutile for Ti; Pyrope garnet for Al and Fe; Rhodonite for Mn; Diopside for Si, Mg, and Ca; Eskolaite for Cr; and Sanidine for K. For experiments at relatively low temperatures (1150–1250 °C), quenched glasses in the pores of carbon spheres were targeted for analysis. An appropriate beam size was chosen for each analysis to avoid the overlap of electron beam with carbon spheres. Melt compositions from all experiments were normalized to 100% for the purpose of comparison.

Attainment of equilibrium

Two pieces of evidence indicate that our run products from high-pressure crystallization/melting experiments have attained equilibrium. First, no systematic variations in mineral compositions were found across the width or length of the experimental charges. Second, the residual sums of squares in the mass balance calculations were small (from 0.05 to 0.90) except for Run #MA21 at the 1150 °C (4.9), which may be out of equilibrium due to low temperature. The Run # MA16 at 1300 °C shows a somewhat different composition trend and mineral fractions trend from other runs at 1350 °C and 1250 °C. This was likely caused by disequilibrium for a short duration.

Parameterized model for deep magma evolution

At the pressure comparable to the base of the lithosphere (~3 GPa), the major element compositions of HP-derived melt after high-pressure crystallization process can be parameterized as functions of melt fraction (MF) or crystallization fraction (CF = 1-MF) based on the experimental results on both CO_2-bearing systems, CP-2 with ~6.6 wt% CO_2 in this study, and those on CO_2-free systems from ref. 16 (Fig. 3). With decreasing temperature or increasing CF, the SiO_2, MgO, and Al_2O_3 contents decrease and FeO^T content increases, whereas the CaO content changes depending on its absolute value in the starting composition. Therefore, we selected four major element components, SiO_2, MgO, FeO^T, and Al_2O_3 for modelling the evolution of magma

chemistry. The normalized contents $\bar{X}_i^{HP-derived}$ (i = SiO_2, MgO, FeO^T, Al_2O_3) as functions of CF can be described as,

$$\bar{X}_i^{HP-derived} = A_i + B_i \times (1 - \mathrm{CF}) + C_i \times (1 - \mathrm{CF})^2 \quad (1)$$

where A_i, B_i, and C_i are further parameterized as linear functions of CO_2 content in the primary magma ($X_{CO_2}^{Pri}$) as follows:

$$A_i = a_i + b_i \times X_{CO_2}^{Pri} \quad (2)$$

$$B_i = c_i + d_i \times X_{CO_2}^{Pri} \quad (3)$$

$$C_i = e_i + f_i \times X_{CO_2}^{Pri} \quad (4)$$

where a_i, b_i, c_i, d_i, e_i, and f_i are fitting parameters. For the MgO component, $\bar{X}_{MgO}^{HP-derived}$ is assumed to be a linear function of CF, and thus e_i and f_i are zero. The fitting results for all parameters in Eqs. (2–4) are listed in Supplementary Table 7. Given the CO_2 content range in the starting materials of this study and those in ref. 16, our model is valid for primary magmas with CO_2 contents from 0 to 6.6 wt%.

The orthopyroxene assimilation is inevitably accompanied by olivine precipitation, which is crucial for determining the composition of the evolved magma. Such olivine precipitation cannot be distinguished from those crystallized at low pressure due to decreasing temperature. We thus consider all olivine precipitation occurs at shallow depths and followed ref. 35 to estimate the parental OIB magma compositions by adding olivine back. Then the melt-orthopyroxene reaction fractions are simplified as the amount of absorbed orthopyroxene in wt%. The calculated major element contents X_i^{Calc} in parental magmas can be solved by mass balance equation as follows:

$$\bar{X}_i^{Calc} = \bar{X}_i^{HP-derived} \times (1 - \mathrm{RF}) + X_i^{Opx} \times \mathrm{RF} \quad (5)$$

where X_i^{Opx} is constant corresponding to the major element contents in orthopyroxene (Supplementary Table 2). Finally, $\bar{X}_i^{Calc}$ can be calculated using Eqs. (1–5) with three variables: CF, RF, and $X_{CO_2}^{Pri}$.

For each natural OIB composition, the parental magma composition estimated in ref. 35 was used as the target composition ($\bar{X}_i^{Target}$) to be compared with model calculations. Defining $\Delta\bar{X}_i$ as the difference between the calculated and target compositions,

$$\Delta\bar{X}_i = \bar{X}_i^{Calc} - \bar{X}_i^{Target} \quad (6)$$

the CF, RF, and $X_{CO_2}^{Pri}$ for each OIB composition can be obtained by minimizing the residual sum of squares (RSS) as

$$\mathrm{RSS} = \sum_{\mathrm{i}} \left(\Delta\bar{X}_i\right)^2 \quad (7)$$

The calculated major element contents for SiO_2, MgO, FeO^T, and Al_2O_3 are compared with target compositions in Supplementary Fig. 7. The calculated SiO_2 contents have the lowest $\Delta\bar{X}_i$ among all four components (with differences less than 3%). The maximal differences of mean compositions of calculated OIBs in individual island are less than 20%.

Data availability

The composition data of MORBs used for comparison in this study are available from the GEOROC database (https://georoc.mpch-mainz.gwdg.de//georoc/). The experimental results and calculations data generated in this study are provided in the Supplementary Information as Supplementary Tables 1–7. These data are also available at https://data.mendeley.com/datasets/bby933t9m8/1.

References

1. Dasgupta, R., Hirschmann, M. M. & Smith, N. D. Partial melting experiments of peridotite + CO_2 at 3 GPa and genesis of alkalic ocean island basalts. *J. Petrol.* **48**, 2093–2124 (2007).
2. Hirose, K. Partial melt compositions of carbonated peridotite at 3 GPa and role of CO_2 in alkali-basalt magma generation. *Geophys. Res. Lett.* **24**, 2837–2840 (1997).
3. Niu, Y. & O'Hara, M. J. Origin of ocean island basalts: a new perspective from petrology, geochemistry, and mineral physics considerations. *J. Geophys. Res.* **108**, 2209 (2003).
4. Brey, G. Origin of olivine melilitites—chemical and experimental constraints. *J. Volcanol. Geotherm. Res.* **3**, 61–88 (1978).
5. Herzberg, C. et al. Phantom Archean crust in Mangaia hotspot lavas and the meaning of heterogeneous mantle. *Earth Planet. Sci. Lett.* **396**, 97–106 (2014).
6. Weiss, Y., Class, C., Goldstein, S. L. & Hanyu, T. Key new pieces of the HIMU puzzle from olivines and diamond inclusions. *Nature* **537**, 666–670 (2016).
7. Mazza, S. E. et al. Sampling the volatile-rich transition zone beneath Bermuda. *Nature* **569**, 398–403 (2019).
8. Hirschmann, M. M., Kogiso, T., Baker, M. B. & Stolper, E. M. Alkalic magmas generated by partial melting of garnet pyroxenite. *Geology* **31**, 481–484 (2003).
9. Kogiso, T., Hirschmann, M. M. & Frost, D. J. High-pressure partial melting of garnet pyroxenite: possible mafic lithologies in the source of ocean island basalts. *Earth Planet. Sci. Lett.* **216**, 603–617 (2003).
10. Dasgupta, R., Hirschmann, M. M. & Stalker, K. Immiscible transition from carbonate-rich to silicate-rich melts in the 3 GPa melting interval of eclogite + CO_2 and genesis of silica-undersaturated ocean island lavas. *J. Petrol.* **47**, 647–671 (2006).
11. Keshav, S., Gudfinnsson, G. H., Sen, G. & Fei, Y. High-pressure melting experiments on garnet clinopyroxenite and the alkalic to tholeiitic transition in ocean-island basalts. *Earth Planet. Sci. Lett.* **223**, 365–379 (2004).
12. Lambart, S., Laporte, D. & Schiano, P. Markers of the pyroxenite contribution in the major-element compositions of oceanic basalts: review of the experimental constraints. *Lithos* **160**, 14–36 (2013).
13. Mallik, A. & Dasgupta, R. Reactive infiltration of MORB-eclogite-derived carbonated silicate melt into fertile peridotite at 3 GPa and genesis of alkalic magmas. *J. Petrol.* **54**, 2267–2300 (2013).
14. Mallik, A. & Dasgupta, R. Effect of variable CO_2 on eclogite-derived andesite and lherzolite reaction at 3 GPa—implications for mantle source characteristics of alkalic ocean island basalts. *Geochem. Geophys. Geosyst.* **15**, 1533–1557 (2014).
15. Mallik, A. & Dasgupta, R. Reaction between MORB-eclogite derived melts and fertile peridotite and generation of ocean island basalts. *Earth Planet. Sci. Lett.* **329-330**, 97–108 (2012).
16. Yang, J., Wang, C., Zhang, J. & Jin, Z. Genesis of Hawaiian lavas by crystallization of picritic magma in the deep mantle. *Nat. Commun.* **14**, 1382 (2023).
17. Miller, L. A., O'Neill, H. S. C., Berry, A. J. & Le Losq, C. Fractional crystallisation of eclogite during the birth of a Hawaiian Volcano. *Nat. Commun.* **13**, 2946 (2022).
18. O'Hara, M. J. & Yoder, H. S. Formation and fractionation of basic magmas at high pressures. *Scott. J. Geol.* **3**, 67–117 (1967).
19. Sen, G. & Jones, R. E. Cumulate xenolith in Oahu, Hawaii: implications for deep magma chambers and Hawaiian volcanism. *Science* **249**, 1154–1157 (1990).

20. Keshav, S., Sen, G. & Presnall, D. C. Garnet-bearing xenoliths from Salt Lake Crater, Oahu, Hawaii: high-pressure fractional crystallization in the oceanic mantle. *J. Petrol.* **48**, 1681–1724 (2007).
21. Kelemen, P. B. Reaction between ultramafic rock and fractionating basaltic magma: I. Phase relations, the origin of calc-alkaline magma series, and the formation of discordant dunite. *J. Petrol.* **31**, 51–98 (1990).
22. Daines, M. J. & Kohlstedt, D. L. The transition from porous to channelized flow due to melt/rock reaction during melt migration. *Geophys. Res. Lett.* **21**, 145–148 (1994).
23. Wagner, T. P. & Grove, T. L. Melt/harzburgite reaction in the petrogenesis of tholeiitic magma from Kilauea volcano, Hawaii. *Contrib. Mineral. Petrol.* **131**, 1–12 (1998).
24. Kelemen, P. B., Hart, S. R. & Bernstein, S. Silica enrichment in the continental upper mantle via melt/rock reaction. *Earth Planet. Sci. Lett.* **164**, 387–406 (1998).
25. Hoernle, K., Tilton, G., Le Bas, M. J., Duggen, S. & Garbe-Schönberg, D. Geochemistry of oceanic carbonatites compared with continental carbonatites: mantle recycling of oceanic crustal carbonate. *Contrib. Mineral. Petrol.* **142**, 520–542 (2002).
26. Saal, A. E., Hart, S. R., Shimizu, N., Hauri, E. H. & Layne, G. D. Pb isotopic variability in melt inclusions from oceanic island basalts, Polynesia. *Science* **282**, 1481–1484 (1998).
27. Neumann, E.-R., Wulff-Pedersen, E., Pearson, N. J. & Spencer, E. A. Mantle xenoliths from Tenerife (Canary islands): dvidence for reactions between mantle peridotites and silicic carbonatite melts inducing Ca metasomatism. *J. Petrol.* **43**, 825–857 (2002).
28. Dalton, J. A. & Wood, B. J. The compositions of primary carbonate melts and their evolution through wallrock reaction in the mantle. *Earth Planet. Sci. Lett.* **119**, 511–525 (1993).
29. Hammouda, T., Chantel, J., Manthilake, G., Guignard, J. & Crichton, W. Hot mantle geotherms stabilize calcic carbonatite magmas up to the surface. *Geology* **42**, 911–914 (2014).
30. Russell, J. K., Porritt, L. A., Lavallée, Y. & Dingwell, D. B. Kimberlite ascent by assimilation-fuelled buoyancy. *Nature* **481**, 352–356 (2012).
31. Kogiso, T., Hirschmann, M. M. & Pertermann, M. High-pressure partial melting of mafic lithologies in the mantle. *J. Petrol.* **45**, 2407–2422 (2004).
32. Brooker, R. A., Kohn, S. C., Holloway, J. R. & McMillan, P. F. Structural controls on the solubility of CO_2 in silicate melts: Part II: IR characteristics of carbonate groups in silicate glasses. *Chem. Geol.* **174**, 241–254 (2001).
33. Rosenthal, A., Hauri, E. H. & Hirschmann, M. M. Experimental determination of C, F, and H partitioning between mantle minerals and carbonated basalt, CO_2/Ba and CO_2/Nb systematics of partial melting, and the CO_2 contents of basaltic source regions. *Earth Planet. Sci. Lett.* **412**, 77–87 (2015).
34. Klaver, M. et al. Titanium-rich basaltic melts on the Moon modulated by reactive flow processes. *Nat. Geosci.* **17**, 118–123 (2024).
35. Sun, C. & Dasgupta, R. Carbon budget of Earth's deep mantle constrained by petrogenesis of silica-poor ocean island basalts. *Earth Planet. Sci. Lett.* **611**, 118135 (2023).
36. Dasgupta, R., Chi, H., Shimizu, N., Buono, A. S. & Walker, D. Carbon solution and partitioning between metallic and silicate melts in a shallow magma ocean: implications for the origin and distribution of terrestrial carbon. *Geochim. Cosmochim. Acta* **102**, 191–212 (2013).
37. Prytulak, J. & Elliott, T. TiO_2 enrichment in ocean island basalts. *Earth Planet. Sci. Lett.* **263**, 388–403 (2007).
38. Lee, C.-T. A., Luffi, P., Plank, T., Dalton, H. & Leeman, W. P. Constraints on the depths and temperatures of basaltic magma generation on Earth and other terrestrial planets using new thermobarometers for mafic magmas. *Earth Planet. Sci. Lett.* **279**, 20–33 (2009).
39. Putirka, K. Excess temperatures at ocean islands: implications for mantle layering and convection. *Geology* **36**, 283–286 (2008).
40. Sobolev, A. V., Hofmann, A. W., Sobolev, S. V. & Nikogosian, I. K. An olivine-free mantle source of Hawaiian shield basalts. *Nature* **434**, 590–597 (2005).
41. Bao, X., Lithgow-Bertelloni, C. R., Jackson, M. G. & Romanowicz, B. On the relative temperatures of Earth's volcanic hotspots and mid-ocean ridges. *Science* **375**, 57–61 (2022).
42. Anderson, D. L. The persistent mantle plume myth. *Aust. J. Earth Sci.* **60**, 657–673 (2013).
43. French, S., Lekic, V. & Romanowicz, B. Waveform tomography reveals channeled flow at the base of the oceanic asthenosphere. *Science* **342**, 227–230 (2013).
44. Saal, A. E., Hauri, E. H., Langmuir, C. H. & Perfit, M. R. Vapour undersaturation in primitive mid-ocean-ridge basalt and the volatile content of Earth's upper mantle. *Nature* **419**, 451–455 (2002).
45. Crisp, J. A. Rates of magma emplacement and volcanic output. *J. Volcanol. Geotherm. Res.* **20**, 177–211 (1984).
46. Plank, T. & Manning, C. E. Subducting carbon. *Nature* **574**, 343–352 (2019).
47. Yang, J., Wang, C. & Jin, Z. Crystallization of hydrous Ti-rich basaltic magma and its implication for the origin of Fe–Ti oxide in layered intrusions of the Emeishan large igneous province. *J. Earth Sci.* **33**, 507–512 (2022).
48. Pickering-Witter, J. & Johnston, A. D. The effects of variable bulk composition on the melting systematics of fertile peridotitic assemblages. *Contrib. Mineral. Petrol.* **140**, 190–211 (2000).
49. Pertermann, M. & Hirschmann, M. M. Partial melting experiments on a MORB-like pyroxenite between 2 and 3 GPa: constraints on the presence of pyroxenite in basalt source regions from solidus location and melting rate. *J. Geophys. Res.* **108**, 2125 (2003).
50. Spandler, C., Yaxley, G., Green, D. H. & Rosenthal, A. Phase relations and melting of anhydrous K-bearing eclogite from 1200 to 1600°C and 3 to 5 GPa. *J. Petrol.* **49**, 771–795 (2008).
51. Beattie, P., Ford, C. & Russell, D. Partition coefficients for olivine-melt and orthopyroxene-melt systems. *Contrib. Mineral. Petrol.* **109**, 212–224 (1991).
52. Walter, M. J. Melting of garnet peridotite and the origin of komatiite and depleted lithosphere. *J. Petrol.* **39**, 29–60 (1998).
53. Davis, F. A., Hirschmann, M. M. & Humayun, M. The composition of the incipient partial melt of garnet peridotite at 3 GPa and the origin of OIB. *Earth Planet. Sci. Lett.* **308**, 380–390 (2011).
54. Marty, B. & Tolstikhin, I. N. CO_2 fluxes from mid-ocean ridges, arcs and plumes. *Chem. Geol.* **145**, 233–248 (1998).

Acknowledgements

This work was partially supported by the National Natural Science Foundation of China (92479108), the High Level Special Fund of SUSTech (G03050K001) to Z.Jing, the National Natural Science Foundation of China (42473043) to C.W., and the China Postdoctoral Science Foundation (2023T160291) to J.Y.

Author contributions

J.Y., C.W., and Z.Jing designed the project. J.Y. conducted the experiments and chemical analyses. J.Y. and Z.Jing performed modelling of the results and co-wrote the manuscript. J.Y., Z.Jing, C.W., and Z.Jin contributed to the discussion of the results and editing of the manuscript.

Competing interests

The authors declare no competing interests.

Additional information

Supplementary information The online version contains supplementary material available at https://doi.org/10.1038/s41467-025-60619-2.

Correspondence and requests for materials should be addressed to Chao Wang or Zhicheng Jing.

Peer review information *Nature Communications* thanks Angelika Rosa, and the other, anonymous, reviewer(s) for their contribution to the peer review of this work. A peer review file is available.